European Journal of Radiology 153 (2022) 110386

Contents lists available at ScienceDirect

European Journal of Radiology

journal homepage: www.elsevier.com/locate/ejrad

Myocardial extracellular volume quantification by cardiac CT in pulmonary hypertension: Comparison with cardiac MRI

Hidetaka Hayashi [a], Seitaro Oda [a,*], Takafumi Emoto [b], Masafumi Kidoh [a], Yasunori Nagayama [a], Takeshi Nakaura [a], Daisuke Sakabe [b], Shinichi Tokuyasu [c], Kyoko Hirakawa [d], Seiji Takashio [d], Eiichiro Yamamoto [d], Kenichi Tsujita [d], Toshinori Hirai [a]

[a] Department of Diagnostic Radiology, Faculty of Life Sciences, Kumamoto University, 1-1-1 Honjyo, Chuo-ku, Kumamoto 860-8556, Japan
[b] Department of Central Radiology, Kumamoto University Hospital, 1-1-1 Honjyo, Chuo-ku, Kumamoto 860-8556, Japan
[c] CT Clinical Science, Philips Japan, Kohnan 2-13-37, Minato-ku, Tokyo 108-8507, Japan
[d] Department of Cardiovascular Medicine, Faculty of Life Sciences, Kumamoto University, 1-1-1 Honjyo, Chuo-ku, Kumamoto 860-8556, Japan

ARTICLE INFO

Keywords:
Myocardial extracellular volume
Pulmonary hypertension
Magnetic resonance imaging
Computed tomography

ABSTRACT

Purpose: Myocardial extracellular volume (ECV) measured by cardiac magnetic resonance imaging (MRI) has been suggested as a marker of disease severity in pulmonary hypertension (PH). However, consistency between ECVs quantified by computed tomography (CT) and MRI has not been sufficiently investigated in (PH). We investigated the utility of CT-ECV in PH, using MRI-ECV as a reference standard.

Method: We evaluated 20 patients with known or suspected PH who underwent dual-energy CT, cardiac MRI, and right heart catheterization. We used Pearson correlation analysis to investigate correlations between CT-ECV and MRI-ECV. We also assessed correlations between ECV and mean pulmonary artery pressure (mPAP).

Results: CT-ECV showed a very strong correlation with MRI-ECV at the anterior ($r = 0.83$) and posterior right ventricular insertion points (RVIPs) ($r = 0.84$). CT-ECV and MRI-ECV were strongly correlated in the septum and left ventricular free wall ($r = 0.79$–0.73) but weakly correlated in the right ventricular free wall ($r = 0.26$). CT-ECV showed a strong correlation with mPAP in the anterior RVIP ($r = 0.64$) and a moderate correlation in the posterior RVIP and septum ($r = 0.50$–0.42). Compared with CT-ECV, MRI-ECV had a higher correlation with mPAP; however, the difference was not significant (anterior RVIP, $r = 0.72$ [MRI-ECV] vs. 0.64 [CT-ECV], $p = 0.663$; posterior RVIP, $r = 0.67$ vs. 0.50, $p = 0.446$).

Conclusion: Dual-energy CT can quantify myocardial ECV and yield results comparable to those obtained using cardiac MRI. CT-ECV in the anterior RVIP could be a noninvasive surrogate marker of disease severity in PH.

1. Introduction

Pulmonary hypertension (PH) is a pathophysiological disorder characterized by the elevation of mean pulmonary artery pressure (mPAP) to 25 mmHg or higher at rest, as assessed by right heart catheterization (RHC) [1]. Increased afterload (pressure overload) causes right ventricular (RV) hypertrophy, dilatation, fibrosis, and eventually heart failure.

Recently, late gadolinium enhancement (LGE) and T1 mapping, myocardial native T1, and extracellular volume fraction (ECV), on cardiac magnetic resonance imaging (MRI) have been receiving attention. These MRI sequences allow us to noninvasively visualize the extent of fibrosis in the myocardium.

Previous research has shown that the imaging biomarkers of cardiac MRI (LGE, native T1, and ECV) are associated with RV function, RV hemodynamics, disease severity, and prognosis in PH [2–7]. However, cardiac MRI has several challenges, including longer acquisition times, limited imaging sections, and lack of applicability to patients who require mechanical device support. Gadolinium-enhanced cardiac MRI is contraindicated in patients undergoing dialysis. Furthermore, it is difficult for patients with heart failure to tolerate acquisitions involving multiple and long breath-holds. In comparison with cardiac MRI, cardiac computed tomography (CT) is widely used because of its accessibility, fast acquisition times, suitability for coronary artery imaging, and

* Corresponding author at: Department of Diagnostic Radiology, Faculty of Life Sciences, Kumamoto University, 1-1-1 Honjo, Chuo-ku, Kumamoto 860-8556, Japan.
E-mail address: seisei0430@nifty.com (S. Oda).

https://doi.org/10.1016/j.ejrad.2022.110386
Received 18 February 2022; Received in revised form 21 May 2022; Accepted 26 May 2022
Available online 30 May 2022

suitability for use in patients with mechanical devices, and those undergoing dialysis. This modality has recently evolved to include myocardial assessment, leading to myocardial characterizations that are comparable to ECV quantification using cardiac MRI [8,9]. Yamasaki et al. recently demonstrated a correlation between CT-ECV and mPAP in chronic thromboembolic PH and concluded that CT-ECV could provide surrogate markers of disease severity and reverse tissue remodeling [10]. This study was the first to report CT-ECV in patients with PH; however, as the authors noted, its validity was not verified by comparison with MRI-ECV.

Therefore, this study aimed to assess the utility of CT-ECV in patients with PH, using MRI-ECV as a reference standard.

2. Materials and methods

2.1. Study population

We retrospectively reviewed the clinical records of patients with known or suspected PH who underwent the comprehensive PH assessment CT scan protocol at our institution between April 2020 and September 2021. This protocol included pulmonary CT angiography, pulmonary perfusion imaging, and myocardial CT-ECV analysis using a dual-energy CT system; it was clinically applied at our institution to patients with known or suspected PH [11]. As physicians wanted information about myocardial impairment due to the coexistence of myocardial infarction and cardiomyopathy, CT-ECV analysis (equilibrium phase image acquisition) was added to our institution. During the study period, 52 patients were referred for the CT scan protocol. Of these, 20 patients also underwent cardiac MRI and RHC within 3 months for clinical reasons based on clinical guidelines (Table 1) [1,12]. Patients with severe image artifacts on either examination were excluded. The study flowchart is shown in Fig. 1. This retrospective study was approved by the institutional review board, who waived the requirement for written informed consent.

2.2. CT image acquisition

All patients were scanned with a dual-layer spectral detector scanner (IQon Spectral CT; Philips Healthcare, Best, Netherlands). Following our protocol, two-phase images were acquired after contrast injection. We obtained CT pulmonary angiography and pulmonary perfusion images during first-phase imaging; equilibrium phase cardiac images for CT-ECV analysis were acquired during second-phase imaging. First-phase imaging was performed with a 20-second intravenous infusion of 550 mgI/kg of iopamidol (Iopamiron 370; Bayer Healthcare, Osaka, Japan). After 7 min, second-phase imaging was performed using a retrospective electrocardiogram (ECG) gated scan with ECG-based tube current modulation (dose right index, 33). The parameters for equilibrium phase cardiac imaging (second-phase imaging) were as follows: detector collimation, 64 × 0.625 mm; tube rotation time, 270 ms; tube voltage, 120 kVp; tube current, 251.6 effective mAs ± 42.1 (range, 208–342 mA); volume CT dose index, 22.8 mGy ± 3.7 (range, 18.8–31 mGy); and dose length product, 431.6 ± 75.4 mGy cm (range, 333.1–607.8 mGy cm). The data acquisition area for equilibrium phase cardiac imaging was set to start at the tracheal carina down to the inferior border of the heart.

The spectral-based image data of the equilibrium phase cardiac images, reconstructed with section thicknesses and intervals of 1.0 mm and 1.0 mm, were post-processed using a dedicated workstation (IntelliSpace Portal version 10.1, Philips Healthcare) to generate iodine density images (spectral level 3). The original data set of 1.0 mm axial images was processed for multiplanar reformation, in the short-axis plane, with a section thickness of 8.0 mm and a section interval of 4.0 mm. To create a myocardial CT-derived ECV map, iodine density images were analyzed using a postprocessing workstation (IntelliSpace Portal version 12.1; Philips Healthcare). The iodine density-derived CT-ECV [8] was calculated as follows: CT-ECV (%) = (1 − hematocrit) × (iodine density in myocardium)/(iodine density in the blood pool) × 100.

Table 1
Patient characteristics.

Number of patients	20
Sex (male/female)	4/16
Age (years)	59.8 ± 16.0
Body height (cm)	158.1 ± 10.3
Body weight (kg)	57.4 ± 15.5
Body surface area (m^2)	1.57 ± 0.23
WHO functional class (I/II/III/IV)	4/11/5/0
PH group (1/2/3/4/5/non)	8/0/0/11/0/1
Past treatment (n)	
Pulmonary vasodilator	3
BPA	3
Anticoagulant	11
ASD repair	1

Data are presented as means ± standard deviation or actual values.
Abbreviations: WHO, World Health Organization; PH, pulmonary hypertension; BPA, balloon pulmonary angioplasty; ASD, atrial septal defect.

2.3. Cardiac MRI acquisition

All cardiac MRI studies were performed using a 3.0-T MRI scanner (Ingenia CX, Philips Healthcare). Patients were scanned in the supine position using a 16-channel phased-array coil. ECG-gated cine images were obtained with a segmented steady-state free precession sequence; moreover, T1 mapping and LGE imaging were performed. For MRI-ECV quantification, pre- and post-contrast (15 min) T1 mapping was performed in a single mid-ventricular short-axis slice (section thickness, 8 mm) using the shortened modified Look–Locker inversion recovery sequence. We used 0.2 mmol/kg of gadolinium-based contrast material (Gadovist; Bayer Yakuhin, Osaka, Japan). MRI-ECV maps were generated using a postprocessing workstation (Ziostation 2 version 2.9; Ziosoft, Tokyo, Japan).

2.4. ECV quantification and data analysis

Quantitative ECV measurements were determined from CT-ECV and MRI-ECV maps. All measurements were independently performed by 2 cardiovascular radiologists (H.H. and S.O.) with 5 years and 15 years of experience, respectively, in cardiac CT/MRI; they had no prior knowledge of the patients' clinical information. The ECVs were measured at the anterior right ventricular insertion point (RVIP), septum, posterior RVIP, left ventricular (LV) free wall, and RV free wall in the LV short-axis view of the mid-ventricular level (Fig. 2). Each myocardial region of interest was manually drawn as large as possible, to include all points while paying attention to avoid the in-plane partial volume effects of blood, epicardial fat, and lung.

2.5. RHC

The transjugular approach was used to perform the standard RHC procedure in free breathing condition in a supine position using a Swan–Ganz catheter. Cardiac output was assessed using thermodilution, and the data obtained comprised systolic, diastolic, and mean pulmonary arterial pressure, pulmonary arterial wedge pressure, right atrial pressure, and pulmonary vascular resistance. Additionally, during RHC, the mean systolic and diastolic blood pressures were assessed.

2.6. Statistical analysis

All numeric values are reported as means ± standard deviation. Differences between mean values from CT-ECV and MRI-ECV were determined using a two-tailed independent *t*-test. Correlation between CT-ECV and MRI-ECV was evaluated using Pearson correlation analysis.

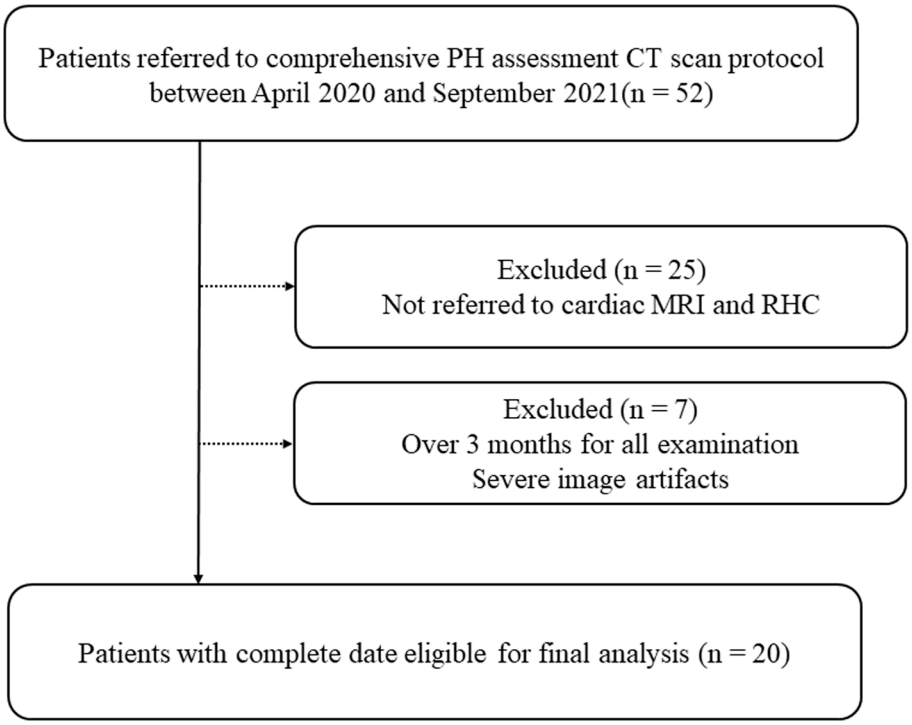

Fig. 1. Study flowchart. Abbreviations: PH, pulmonary hypertension; CT, computed tomography; MRI; magnetic resonance imaging; RHC, right heart catheterization.

For the absolute correlation coefficient values, we considered 0–0.19 as very weak, 0.2–0.39 as weak, 0.40–0.59 as moderate, 0.6–0.79 as strong, and 0.8–1 as very strong correlation values. For assessments of the clinical utility of CT-ECV and MRI-ECV, correlation between the ECV and mPAP (measured in RHC) and LV and RV ejection fraction determined from the cine MRI was also tested using Pearson correlation analysis. The intraclass correlation coefficient (ICC) was calculated in order to determine the level of interobserver agreement for quantification of myocardial ECV. The level of agreement was considered excellent at an ICC $>$ 0.90, good at ICC = 0.75–0.90, moderate at ICC = 0.50–0.74, and poor at ICC $<$ 0.50 [13]. A p-value of $<$ 0.05 was considered statistically significant. All statistical analyses were performed using Bell Curve for Excel (Social Survey Research Information, Tokyo, Japan).

3. Results

3.1. Patient characteristics

The characteristics of the 20 patients (16 women and 4 men; age, 59.8 ± 16.0 years) are summarized in Table 1. The final diagnosis included the following groups: Group 1 (pulmonary arterial hypertension, n = 8); Group 2 (PH due to left heart disease, n = 0); Group 3 (PH due to lung disease and/or hypoxia, n = 0); Group 4 (chronic thromboembolic PH, n = 11); Group 5 (PH with unclear multifactorial mechanisms, n = 0); and Other (n = 1). The patients' New York Heart Association functional classes were Class I, n = 4; Class II, n = 11; Class III, n = 5; and Class IV, n = 0. The average interval between CT and MRI was 10.3 ± 14.6 days (median, 5 days; range, 0–51 days), whereas that between CT and RHC was 6.7 ± 11.7 days (median, 3 days; range, 0–43 days). The mean interval between hematocrit acquisition and imaging was 1.5 ± 1.6 days (range, 0–6 days) for CT and 1.7 ± 2.5 days (range, 0–9 days) for MRI. The mean heart rates were 70.4 ± 10.1 bpm and 69.2 ± 10.3 bpm during CT and MRI, respectively, which were not significantly different.

3.2. Comparison of the CT-ECV and MRI-ECV

CT-ECV was significantly greater than MRI-ECV at the anterior RVIP (35.7% ± 6.2% vs. 33.6% ± 5.7%; p = 0.013), septum (32.0% ± 5.6% vs. 29.9% ± 4.5%; p = 0.011), and LV free wall (31.6% ± 4.5% vs. 29.5% ± 3.8%; p = 0.008).

There were no significant differences between CT-ECV and MRI-ECV at the posterior RVIP (35.4% ± 5.8% vs. 34.7% ± 5.1%; p = 0.340) or the RV free wall (37.0% ± 5.6% vs. 36.7% ± 5.7%; p = 0.839) (Table 2).

3.3. Correlations between CT-ECV and MRI-ECV

CT-ECV showed a very strong correlation with MRI-ECV at the anterior (r = 0.83) and posterior RVIP (r = 0.84). A strong correlation was observed at the septum and LV free wall (r = 0.79–0.73). A weak correlation was shown at the RV free wall (r = 0.26). (Fig. 3). Fig. 4 shows a representative case.

3.4. Correlations of ECV and mPAP with LV and RV ejection fractions

CT-ECV showed a strong correlation with mPAP at the anterior RVIP (r = 0.64) and a moderate correlation at the posterior RVIP and septum (r = 0.50–0.42). Compared with CT-ECV, MRI-ECV had a higher correlation with mPAP; however, the difference was not significant (anterior RVIP, r = 0.72 [MRI-ECV] vs. 0.64 [CT-ECV], p = 0.663; posterior RVIP, r = 0.67 vs. 0.50, p = 0.446) (Table 3). The RV ejection fraction showed a significant negative correlation with both CT-ECV and MRI-ECV, but LVEF did not (Table 4).

3.5. Reliability of ECV measurement

The ICCs for interobserver variability in CT-ECV were 0.95 at the anterior RVIP, 0.95 at the posterior RVIP, 0.95 at the septum, 0.85 at the LV free wall, and 0.68 at the RV free wall. All the ICCs in CT-ECV measurement were classified as excellent, except that of the RV free wall, which was classified as good.

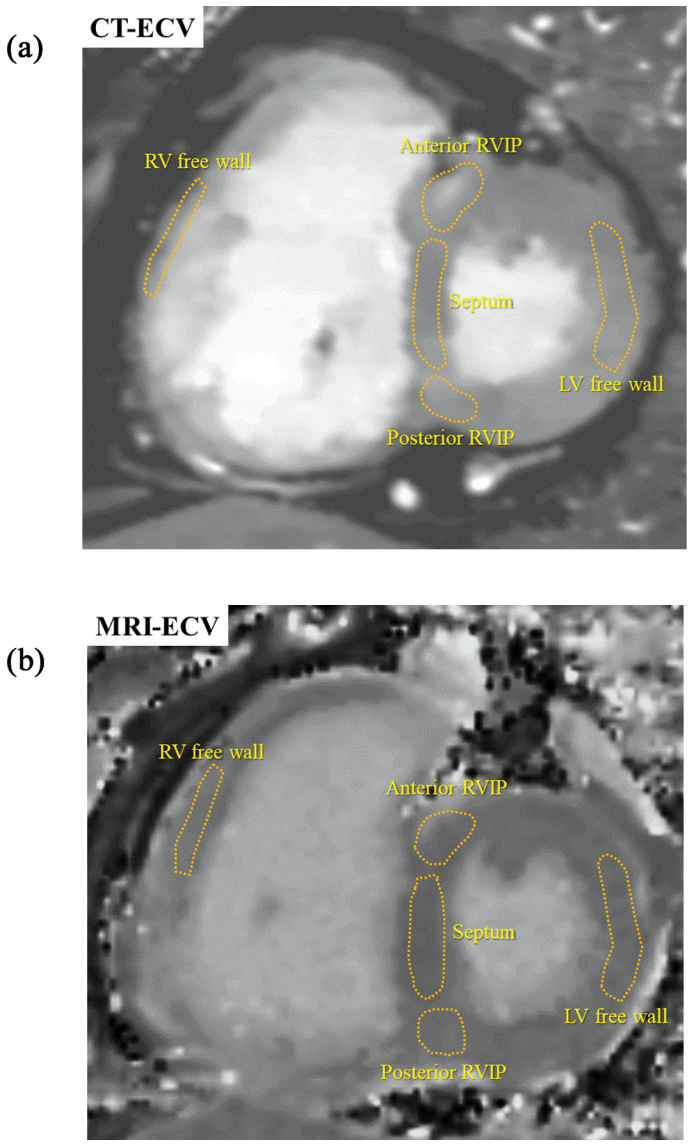

Fig. 2. Quantitative extracellular volume fraction (ECV) measurements. Quantitative ECV measurements were performed using (A) a computed tomography (CT) ECV map and (B) a magnetic resonance imaging (MRI) ECV map. The ECVs were measured at the anterior right ventricular insertion point (RVIP), septum, LV posterior RVIP, left ventricular (LV) free wall, and right ventricle (RV) free wall in the LV short-axis view of the mid-ventricular level.

Table 2
Comparison of CT-ECV and MRI-ECV.

Segment	CT-ECV (%)	MRI-ECV (%)	p-value
Anterior RVIP	35.7 ± 6.2	33.6 ± 5.7	0.013
Posterior RVIP	35.4 ± 5.8	34.7 ± 5.1	0.340
Septum	32.0 ± 5.6	29.9 ± 4.5	0.011
LV free wall	31.6 ± 4.5	29.5 ± 3.8	0.008
RV free wall	37.0 ± 5.6	36.7 ± 5.7	0.839
Global-LV	33.7 ± 5.1	31.9 ± 4.4	0.008

Abbreviations: CT, computed tomography; MRI, magnetic resonance imaging; ECV, extracellular volume; LV, left ventricular; RV, right ventricular; RVIP, right ventricular insertion point.

The ICC for interobserver variability in MRI-ECV was 0.95 at the anterior RVIP, 0.88 at the posterior RVIP, 0.91 at the septum, 0.90 at the LV free wall, and 0.82 at the RV free wall. All the ICCs for MRI-ECV measurements were classified between good and excellent.

4. Discussion

We found a very strong correlation between CT-ECV and MRI-ECV at the anterior and posterior RVIP (r = 0.83–0.84). A strong correlation was observed at the septum and LV free wall (r = 0.79–0.73). Although MRI-ECV had a higher correlation with mPAP than did CT-ECV (anterior RVIP, r = 0.72; posterior RVIP, r = 0.67), CT-ECV showed a strong correlation with mPAP at the anterior RVIP (r = 0.64), and a moderate correlation at the posterior RVIP and septum (r = 0.50–0.42). Thus, CT-ECV provided information about myocardial tissue characterization that was comparable with MRI-ECV. CT-ECV could be a noninvasive surrogate marker of disease severity in patients with PH.

It is well-known that myocardial fibrosis is a common final pathway in almost every heart disease irrespective of its etiology. RV fibrosis can be visually observed using LGE imaging in cardiac MRI [1]. A recent study by Kim et al. investigated the feasibility of T1 mapping in cardiac MRI for evaluating the progression of myocardial fibrosis in PH. They compared the T1 mapping findings to histological collagen density, determined through an animal study [14]. They revealed significantly increased native T1 and ECV of the RV wall, according to the disease

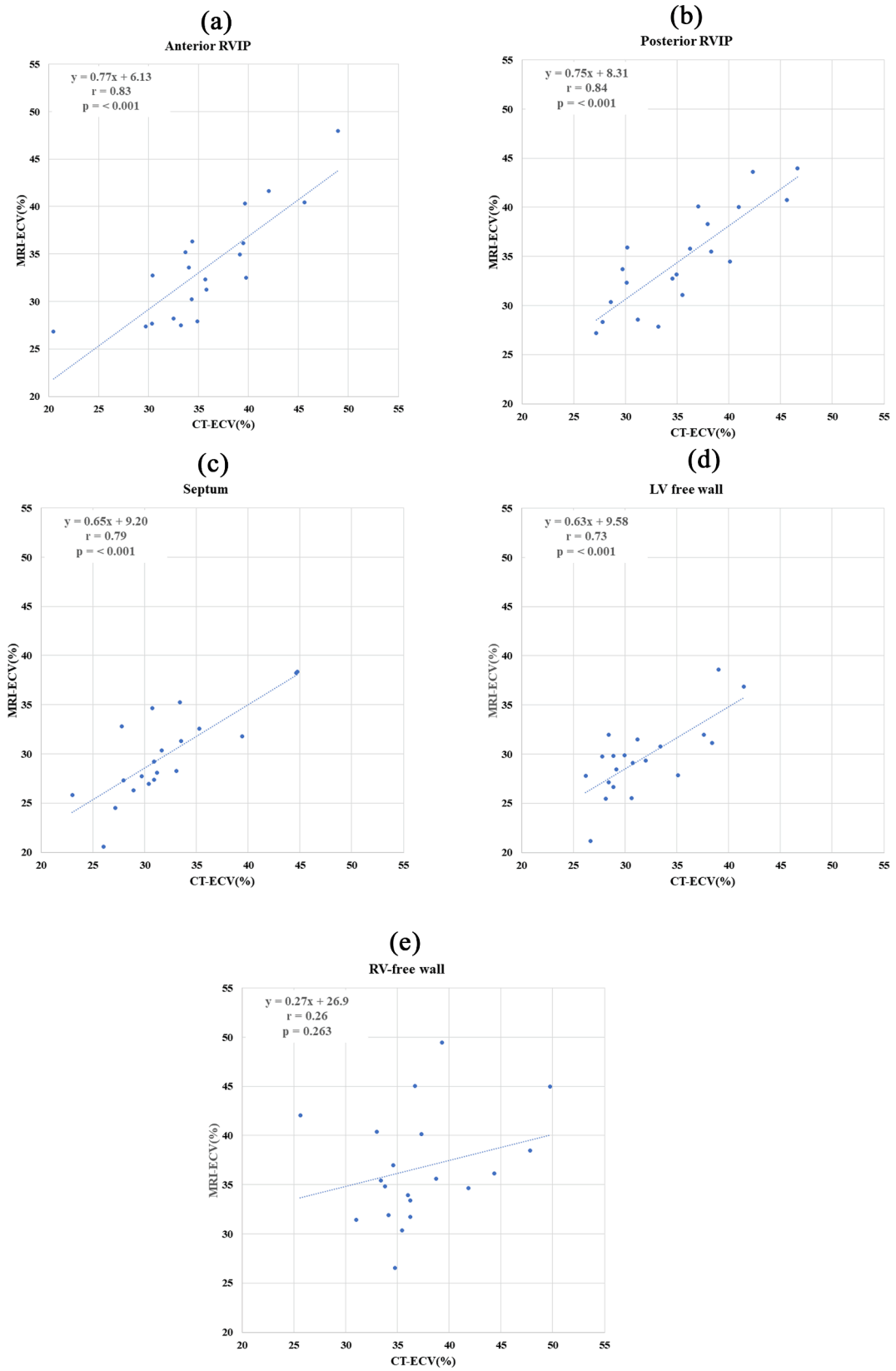

Fig. 3. Correlations between CT-ECV and MRI-ECV. CT-ECV showed a very strong correlation with MRI-ECV in (A) the anterior RVIP (r = 0.83) and (B) the posterior RVIP (r = 0.84). Strong correlation was observed in (C) the septum (r = 0.79) and (D) the LV free wall (r = 0.73). Weak correlation was shown in (E) the RV free wall (r = 0.26).Abbreviations: CT, computed tomography; MRI, magnetic resonance imaging; ECV, extracellular volume fraction; LV, left ventricular; RV, right ventricular; RVIP, right ventricular insertion point.

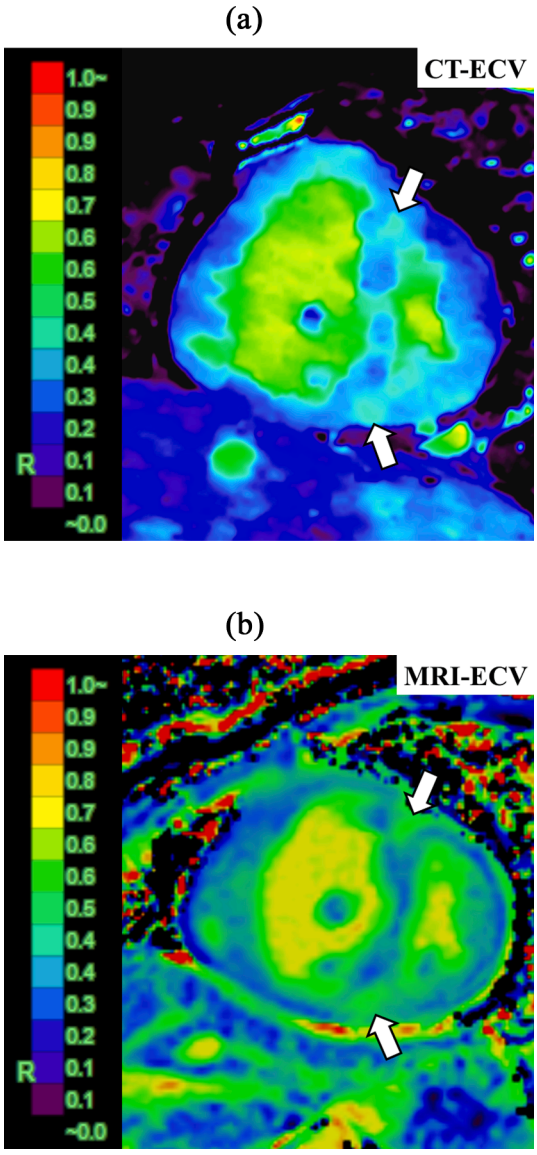

Fig. 4. A representative case. (A) Computed tomography (CT)-derived extracellular volume (ECV) and (B) cardiac magnetic resonance imaging (MRI)-derived ECV in a 38-year-old woman with idiopathic pulmonary arterial hypertension. CT-ECV and MRI-ECV images show significantly elevated myocardial ECV, especially in the anterior and posterior RVIP (arrows). The values of ECV at the anterior and posterior right ventricular insertion point were 48.9% and 46.6%, respectively, for CT-ECV, and 47.9% and 44.0%, respectively, for MRI-ECV. CT-derived ECV and cardiac MRI-derived ECV quantifications were comparable.

duration of PH; these findings were well correlated with histological collagen density. Thus, T1 mapping and LGE imaging in cardiac MRI enable noninvasive evaluation of myocardial tissue and fibrosis. In particular, ECV, which is a quantitative index, is envisaged to become an imaging biomarker for PH because of its superior sensitivity, reproducibility, and versatility for detecting lesions [15].

Measurement of mPAP by RHC is required for definitive diagnosis of PH; it is also used for disease monitoring and evaluation of treatment effect. However, since this measurement is invasive, it is desirable to establish a noninvasive imaging biomarker that reflects mPAP. Researchers have previously evaluated the correlation between mPAP and imaging biomarkers of cardiac MRI. LGE was commonly observed in the RVIP in 41%–100% of patients with PH; 26%–33% of these patients also had LGE in the septum [16–20]. Previous reports have shown a strong or moderate correlation between LGE (mass or volume) and mPAP [2,3,20,21], whereas some studies showed no correlation [19,22]. Freed et al. reported that PH patients with positive LGE findings had higher mPAP and lower RV ejection fraction, compared with LGE-negative PH patients. Some studies found positive LGE to be associated with worse outcomes in PH patients [17,23].

In terms of T1 mapping in cardiac MRI, it has been reported that native T1 and ECV in the RVIP and septum are higher in PH patients than in healthy control subjects, and associated with poor RV function and RV dilatation [5]. Roller et al. reported a moderate, significant positive correlation between native T1 and mPAP, and a moderate, significant negative correlation between native T1 and RV ejection fraction [4]. Garcia-Alcarez et al. reported a moderate significant correlation between ECV and mPAP in an animal PH model [15]. Recently, Yamasaki et al. evaluated ECV obtained from dual-layer spectral detector CT in PH patients. They reported that CT-ECV in the RVIP and septum were highly correlated with mPAP (septum: $r = 0.61$, $p < 0.001$; mean RVIP: $r = 0.66$, $p < 0.001$) [10]. This study implied that CT-ECV could provide information comparable with MRI-ECV in patients with PH, for noninvasive prediction of mPAP. However, it did not perform comparisons with MRI-ECV. The clinical introduction of CT-ECV requires prior validation against MRI-ECV. To our knowledge, ours is the first study to simultaneously evaluate MRI-ECV, CT-ECV, and mPAP in patients with PH. Our study confirmed that CT-ECV had a very strong correlation with MRI-ECV in the anterior and posterior RVIP ($r = 0.83$–0.84), and that CT-ECV at the anterior RVIP showed a strong correlation with mPAP ($r = 0.64$). The RVIP is believed to be particularly prone to developing fibrosis due to face traction, compression, and shear forces [15,24]; thus, it should reflect the severity of PH. This may be the reason why CT-ECV at the RVIP, especially at the anterior RVIP, strongly correlated with

Table 3
Correlations between ECV and mPAP.

	CT-ECV(r)	p-value	MRI-ECV(r)	p-value	p-value, correlation coefficient comparisons
Anterior RVIP	0.64	0.002	0.72	<0.001	0.663
Posterior RVIP	0.50	0.026	0.67	0.001	0.446
Septum	0.42	0.062	0.48	0.032	0.826
LV free wall	0.02	0.942	0.47	0.039	0.153
RV free wall	0.002	0.993	−0.18	0.459	0.591
Global-LV	0.46	0.042	0.66	0.002	0.389

Abbreviations: ECV, extracellular volume; mPAP, mean pulmonary artery pressure; LV, left ventricular; RV, right ventricular; RVIP, right ventricular insertion point.

Table 4
Correlations between ECV and LV and RV ejection fractions.

	CT-ECV(r)	p-value	MRI-ECV(r)	p-value
LV ejection fraction				
Anterior RVIP	−0.08	0.744	−0.01	0.975
Posterior RVIP	−0.15	0.533	−0.17	0.470
Septum	−0.11	0.479	0.05	0.845
LV free wall	0.07	0.778	−0.09	0.718
RV free wall	−0.04	0.871	−0.13	0.598
Global-LV	−0.08	0.731	−0.06	0.803
RV ejection fraction				
Anterior RVIP	−0.62	0.004	−0.57	0.009
Posterior RVIP	−0.61	0.005	−0.68	0.001
Septum	−0.57	0.009	−0.41	0.071
LV free wall	−0.39	0.087	−0.55	0.011
RV free wall	−0.17	0.464	−0.33	0.150
Global-LV	−0.60	0.005	−0.61	0.004

Abbreviations: ECV, extracellular volume; LV, left ventricular; RV, right ventricular; RVIP, right ventricular insertion point.

mPAP. Although MRI-ECV had a higher correlation with mPAP, CT-ECV can provide adequate myocardial evaluation, comparable with MRI-ECV. CT-ECV could be useful and practical in clinical practice, as an alternative to MRI-ECV.

ECV measurement using cardiac CT has been validated in recent years. It has demonstrated excellent agreement with MRI-ECV in patients with LV heart disease [8,9,25,26]. However, the accuracy of CT-ECV in PH, which has RV dominant fibrosis as its main pathological condition, has not been properly investigated. According to our results, CT-ECV at the anterior RVIP most accurately reflected the severity of PH. It also showed a good correlation with MRI-ECV. Thus, it may be an optimal imaging biomarker in PH. We found no significant correlation between CT-ECV in the RV free wall and mPAP. In contrast, Yamasaki et al. reported that the CT-ECV in the RV free wall was moderately correlated with mPAP [10]. Our CT-ECV techniques may be limited by resolution issues because of the thinness of the RV wall, which is also susceptible to partial volume effects. An improved resolution, optimization, and standardization of CT-ECV scan protocols are needed to obtain reliable and reproducible RV measurements.

There are some inherent problems in comparing CT-ECV with MRI-ECV. Although cardiac MRI is considered the *gold standard*, is not always accurate for assessing ECV, due to the presence of susceptibility artifacts, motion artifacts, partial volume effects, and misregistration of component images. A previously-published position paper recommended that MRI-ECV measurements should be performed in the septum to ensure accurate assessment in patients with diffuse myocardial disease [27]. In CT-ECV, it has been reported that measurement in the septum (including the RVIP) is the most accurate and correlates better with MRI-ECV than other sites [9,28]. Thus, measurement in the septum and RVIP is considered appropriate for CT-ECV quantification in patients with PH. Dual-energy CT, as used in this study, enables comprehensive evaluation of patients with suspected PH, using CT pulmonary angiography, pulmonary perfusion imaging with myocardial late enhancement, and ECV analysis [11]. We believe that CT offers a practical and useful approach for a noninvasive, *one-stop shop* evaluation of PH.

Our study has several limitations. First, it included a small number of patients and was performed at a single center; thus, selection bias may have occurred. Furthermore, we could not include a control group for comparison. Large-scale, prospective clinical studies are required for rigorous evaluation of the feasibility of our methods. Second, we did not examine the relationship between myocardial ECV results and clinical classifications of PH because the sample size was too small for meaningful comparative analysis. Comparative studies are needed, with a sufficient number of cases to define the CT-ECV features of each type of PH. Third, CT and MRI were performed on different days in almost all patients, which could have affected the results. Fourth, the results were obtained using a detector-based dual-energy system (i.e., dual-layer spectral detector CT scanner) from a single CT vendor; further evaluation should be conducted using tube-based dual-energy CT systems (e.g., dual-source or fast-kVp switching systems). Finally, additional radiation exposure was required to obtain the CT-ECV results. Further reduction of radiation exposure is desirable, but we need to ensure that this can be accomplished without sacrificing image quality.

5. Conclusion

In conclusion, dual-energy CT can quantify myocardial ECV and yield results comparable with those obtained using cardiac MRI. CT-ECV in the anterior RVIP could serve as a noninvasive surrogate marker of disease severity in PH.

Declaration of Competing Interest

Mr. Shinichi Tokuyasu is an employee of Philips Japan. Dr. Masafumi Kidoh belongs to the endowed department at Kumamoto University funded by donations from Philips Japan. The remaining authors have no conflict of interest.

References

[1] N. Galiè, M. Humbert, J.-L. Vachiery, S. Gibbs, I. Lang, A. Torbicki, G. Simonneau, A. Peacock, A.V. Noordegraaf, M. Beghetti, A. Ghofrani, M.A.G. Sanchez, G. Hansmann, W. Klepetko, P. Lancellotti, M. Matucci, T. McDonagh, L.A. Pierard, P.T. Trindade, M. Zompatori, M. Hoeper, 2015 ESC/ERS Guidelines for the Diagnosis and Treatment of Pulmonary Hypertension, Revista Española de Cardiología (English Edition) 69 (2) (2016) 177, https://doi.org/10.1016/j.rec.2016.01.002.

[2] M.L. Shehata, D. Lossnitzer, J. Skrok, D. Boyce, N. Lechtzin, S.C. Mathai, R. E. Girgis, N. Osman, J.A. Lima, D.A. Bluemke, P.M. Hassoun, J. Vogel-Claussen, Myocardial delayed enhancement in pulmonary hypertension: pulmonary hemodynamics, right ventricular function, and remodeling, AJR Am. J. Roentgenol. 196 (1) (2011) 87–94.

[3] T. Sato, I. Tsujino, H. Ohira, N. Oyama-Manabe, Y.M. Ito, T. Noguchi, A. Yamada, D. Ikeda, T. Watanabe, M. Nishimura, R.E. Morty, Paradoxical interventricular septal motion as a major determinant of late gadolinium enhancement in ventricular insertion points in pulmonary hypertension, PloS one 8 (6) (2013) e66724, https://doi.org/10.1371/journal.pone.0066724.

[4] F.C. Roller, C. Wiedenroth, A. Breithecker, C. Liebetrau, E. Mayer, C. Schneider, A. Rolf, C. Hamm, G.A. Krombach, Native T1 mapping and extracellular volume fraction measurement for assessment of right ventricular insertion point and septal fibrosis in chronic thromboembolic pulmonary hypertension, Eur. Radiol. 27 (5) (2017) 1980–1991.

[5] S. Alabed, L. Saunders, P. Garg, Y. Shahin, F. Alandejani, A. Rolf, V.O. Puntmann, E. Nagel, J.M. Wild, D.G. Kiely, A.J. Swift, Myocardial T1-mapping and extracellular volume in pulmonary arterial hypertension: A systematic review and meta-analysis, Magn. Reson. Imaging 79 (2021) 66–75.

[6] C. Nitsche, A.A. Kammerlander, C. Binder, F. Duca, S. Aschauer, M. Koschutnik, A. Snidat, D. Beitzke, C. Loewe, D. Bonderman, C. Hengstenberg, J. Mascherbauer, Native T1 time of right ventricular insertion points by cardiac magnetic resonance: relation with invasive haemodynamics and outcome in heart failure with preserved ejection fraction, Eur. Heart J. Cardiovasc. Imaging 21 (6) (2020) 683–691.

[7] R.B. Patel, E. Li, B.C. Benefield, S.A. Swat, V.B. Polsinelli, J.C. Carr, S.J. Shah, M. Markl, J.D. Collins, B.H. Freed, Diffuse right ventricular fibrosis in heart failure with preserved ejection fraction and pulmonary hypertension, ESC Heart Failure 7 (1) (2020) 254–264.

[8] S. Oda, T. Emoto, T. Nakaura, M. Kidoh, D. Utsunomiya, Y. Funama, Y. Nagayama, S. Takashio, M. Ueda, T. Yamashita, K. Tsujita, Y. Ando, Y. Yamashita, Myocardial Late Iodine Enhancement and Extracellular Volume Quantification with Dual-Layer Spectral Detector Dual-Energy Cardiac CT, Radiol. Cardiothoracic Imaging 1 (1) (2019) e180003, https://doi.org/10.1148/ryct.2019180003.

[9] T. Emoto, M. Kidoh, S. Oda, T. Nakaura, Y. Nagayama, A. Sasao, Y. Funama, S. Araki, S. Takashio, K. Sakamoto, E. Yamamoto, K. Kaikita, K. Tsujita, Y. Yamashita, Myocardial extracellular volume quantification in cardiac CT: comparison of the effects of two different iterative reconstruction algorithms with MRI as a reference standard, Eur. Radiol. 30 (2) (2020) 691–701.

[10] Y. Yamasaki, K. Abe, T. Kamitani, K. Sagiyama, T. Hida, K. Hosokawa, Y. Matsuura, K. Hioki, M. Nagao, H. Yabuuchi, K. Ishigami, Right Ventricular Extracellular Volume with Dual-Layer Spectral Detector CT: Value in Chronic Thromboembolic Pulmonary Hypertension, Radiology 298 (3) (2021) 589–596.

[11] S. Oda, M. Kidoh, Y. Nagayama, T. Nakaura, K. Hirakawa, E. Yamamoto, K. Tsujita, T. Hirai, Non-Invasive Imaging in Pulmonary Hypertension - Comprehensive Assessment Using Dual-Layer Spectral Computed Tomography, Circ. J. 85 (3) (2021) 316, https://doi.org/10.1253/circj.CJ-20-1007.

[12] K. Fukuda, H. Date, S. Doi, Y. Fukumoto, N. Fukushima, M. Hatano, H. Ito, M. Kuwana, H. Matsubara, S.-I. Momomura, M. Nishimura, H. Ogino, T. Satoh, H. Shimokawa, K. Yamauchi-Takihara, K. Tatsumi, H. Ishibashi-Ueda, N. Yamada, S. Yoshida, K. Abe, A. Ogawa, T. Ogo, T. Kasai, M. Kataoka, T. Kawakami, S. Kogaki, M. Nakamura, T. Nakayama, M. Nishizaki, K. Sugimura, N. Tanabe, I. Tsujino, A. Yao, T. Akasaka, M. Ando, T. Kimura, T. Kuriyama, N. Nakanishi, T. Nakanishi, H. Tsutsui, Guidelines for the Treatment of Pulmonary Hypertension (JCS 2017/JPCPHS 2017), Circ. J. 83 (4) (2019) 842–945.

[13] T.K. Koo, M.Y. Li, A Guideline of Selecting and Reporting Intraclass Correlation Coefficients for Reliability Research, J. Chiropractic Med. 15 (2) (2016) 155–163.

[14] P.K. Kim, Y.J. Hong, H.S. Shim, D.J. Im, Y.J. Suh, K.H. Lee, J. Hur, Y.J. Kim, B. W. Choi, H.J. Lee, Serial T1 mapping of right ventricle in pulmonary hypertension: comparison with histology in an animal study, Journal of cardiovascular magnetic resonance : official journal of the Society for Cardiovascular Magnetic, Resonance 23 (1) (2021) 64.

[15] A. García-Álvarez, I. García-Lunar, D. Pereda, R. Fernández-Jimenez, J. Sánchez-González, J.G. Mirelis, M. Nuño-Ayala, D. Sánchez-Quintana, L. Fernández-Friera, J.M. García-Ruiz, G. Pizarro, J. Agüero, P. Campelos, M. Castellá, M. Sabaté, V. Fuster, J. Sanz, B. Ibañez, Association of myocardial T1-mapping CMR with hemodynamics and RV performance in pulmonary hypertension, JACC, Cardiovasc. Imaging 8 (1) (2015) 76–82.

[16] R. Homsi, J.A. Luetkens, D. Skowasch, C. Pizarro, A.M. Sprinkart, J. Gieseke, J. Meyer Zur Heide Gen Meyer-Arend, H.H. Schild, C.P. Naehle, Left Ventricular Myocardial Fibrosis, Atrophy, and Impaired Contractility in Patients With Pulmonary Arterial Hypertension and a Preserved Left Ventricular Function: A Cardiac Magnetic Resonance Study, J. Thoracic Imaging 32(1) (2017) 36-42.

[17] A.J. Swift, S. Rajaram, D. Capener, C. Elliot, R. Condliffe, J.M. Wild, D.G. Kiely, LGE patterns in pulmonary hypertension do not impact overall mortality, JACC, Cardiovasc. Imaging 7 (12) (2014) 1209–1217.
[18] S. Hsu, B.A. Houston, E. Tampakakis, A.C. Bacher, P.S. Rhodes, S.C. Mathai, R. L. Damico, T.M. Kolb, L.K. Hummers, A.A. Shah, Z. McMahan, C.P. Corona-Villalobos, S.L. Zimmerman, F.M. Wigley, P.M. Hassoun, D.A. Kass, R.J. Tedford, Right Ventricular Functional Reserve in Pulmonary Arterial Hypertension, Circulation 133 (24) (2016) 2413–2422.
[19] G.P. McCann, C.T. Gan, A.M. Beek, H.W.M. Niessen, A.V. Noordegraaf, A.C. van Rossum, Extent of MRI delayed enhancement of myocardial mass is related to right ventricular dysfunction in pulmonary artery hypertension, AJR, Am. J. Roentgenol. 188 (2) (2007) 349–355.
[20] K.G. Blyth, B.A. Groenning, T.N. Martin, J.E. Foster, P.B. Mark, H.J. Dargie, A. J. Peacock, Contrast enhanced-cardiovascular magnetic resonance imaging in patients with pulmonary hypertension, Eur. Heart J. 26 (19) (2005) 1993–1999.
[21] J. Sanz, S. Dellegrottaglie, M. Kariisa, R. Sulica, M. Poon, T.P. O'Donnell, D. Mehta, V. Fuster, S. Rajagopalan, Prevalence and correlates of septal delayed contrast enhancement in patients with pulmonary hypertension, Am. J. Cardiol. 100 (4) (2007) 731–735.
[22] F.P. Junqueira, R. Macedo, A.C. Coutinho, R. Loureiro, P.V. De Pontes, R. C. Domingues, E.L. Gasparetto, Myocardial delayed enhancement in patients with pulmonary hypertension and right ventricular failure: evaluation by cardiac MRI, Br. J. Radiol. 82 (982) (2009) 821–826.
[23] B.H. Freed, M. Gomberg-Maitland, S. Chandra, V. Mor-Avi, S. Rich, S.L. Archer, E. B. Jamison Jr., R.M. Lang, A.R. Patel, Late gadolinium enhancement cardiovascular magnetic resonance predicts clinical worsening in patients with pulmonary hypertension, J. Cardiovasc. Magn. Resonance: Off. J. Soc. Cardiovasc. Magn. Resonance 14 (1) (2012) 11.
[24] W.M. Bradlow, R. Assomull, P.J. Kilner, J.S.R. Gibbs, M.N. Sheppard, R. H. Mohiaddin, Understanding late gadolinium enhancement in pulmonary hypertension, Circulation. Cardiovasc. Imaging 3 (4) (2010) 501–503.
[25] R. Wang, X. Liu, U.J. Schoepf, M. van Assen, I. Alimohamed, L.P. Griffith, T. Luo, Z. Sun, Z. Fan, L. Xu, Extracellular volume quantitation using dual-energy CT in patients with heart failure: Comparison with 3T cardiac MR, Int. J. Cardiol. 268 (2018) 236–240.
[26] Y. Ohta, J. Kishimoto, S. Kitao, H. Yunaga, N. Mukai-Yatagai, S. Fujii, K. Yamamoto, T. Fukuda, T. Ogawa, Investigation of myocardial extracellular volume fraction in heart failure patients using iodine map with rapid-kV switching dual-energy CT: Segmental comparison with MRI T1 mapping, J. Cardiovasc. Comput. Tomogr. 14 (4) (2020) 349–355.
[27] D.R. Messroghli, J.C. Moon, V.M. Ferreira, L. Grosse-Wortmann, T. He, P. Kellman, J. Mascherbauer, R. Nezafat, M. Salerno, E.B. Schelbert, A.J. Taylor, R. Thompson, M. Ugander, R.B. van Heeswijk, M.G. Friedrich, Clinical recommendations for cardiovascular magnetic resonance mapping of T1, T2, T2* and extracellular volume: A consensus statement by the Society for Cardiovascular Magnetic Resonance (SCMR) endorsed by the European Association for Cardiovascular Imaging (EACVI), J. Cardiovasc. Magn. Resonance: Off. J. Soc. Cardiovasc. Magn. Resonance 19 (1) (2017) 75.
[28] T. Emoto, S. Oda, M. Kidoh, T. Nakaura, Y. Nagayama, D. Sakabe, K. Kakei, M. Goto, Y. Funama, M. Hatemura, S. Takashio, K. Kaikita, K. Tsujita, O. Ikeda, Myocardial Extracellular Volume Quantification Using Cardiac Computed Tomography: A Comparison of the Dual-energy Iodine Method and the Standard Subtraction Method, Acad. Radiol. 28 (5) (2021) e119–e126.